Modeling of Galaxies

Sílvia Casacuberta Puig

Abstract

Using data from the Updated Nearby Galaxy Catalog by the Astrophysics Science Division at NASA, we compare the radii, rotation velocity, luminosity and mass of different morphological types of galaxies. We calculate the percentage of missing mass and the value of the constant a_0 of the Modified Newtonian Dynamics formula. We explain the influence of dark matter and why flat rotation curves appear. We present several models commonly used to simulate galaxies and fit their parameters to the data we have collected in this study. Finally we discuss the possible candidates for dark matter.

Key words: galaxies kinematics - dark matter - methods: data analysis

1 Introduction

For centuries scientists have tried to unveil mathematical rules followed by nature. The rotational velocity of planets was explained by means of Kepler's laws, which helped Newton to postulate his formulae. However, the rotational velocities of spiral galaxies are not inversely proportional to their radii and hence do not agree with Kepler's and Newton's formulation. Further investigations (Persic et al. 1996) showed that most galaxies follow a flat rotation curve. This behaviour can only be explained by the presence of an extra source of gravity (i.e., dark matter) or if equations for gravity are wrong or incomplete.

From observations of galaxies we only have luminosity-velocity data. To get the real mass distribution, and therewith confirm that additional matter to the luminous one is needed, we have to assume an analytical model for the gravitational potential and fit the data to it. Therefore, several models have been proposed. The five most famous models are the uniform sphere, the isothermal sphere, the Plummer model, the Henriquist model, and the Jaffe model.

Moreover, the Modified Newtonian Dynamics (MOND) proposed by Milgrom (2005) provide an alternative to dark matter. We also explain the classification of galaxies according to their morphology and describe the theoretical Keplerian velocity profile of galaxies. Once we present how measurements of velocity profiles are made on galaxies, we explain the existence of missing mass and the observed flat rotation curves. MOND theory is one example of the effort that has been made to obtain a new theory for gravity. The MOND approach is valid only for very low accelerations, which is the case of flat rotation curves, but not to explain general processes of galaxy formation and evolution.

Afterwards, using data from the Updated Nearby Galaxy Catalog by the Astrophysics Science Division at NASA, we analyze data of radii, velocity, luminosity and mass within the Holmberg radius (Bosma 2016) for 91 galaxies of several morphological types. We then calculate other parameters: the mass/luminosity ratio, the difference between the Keplerian predicted velocity and the real one, the constant a_0 for the Modified Newtonian Dynamics and the percentage of missing mass. Finally, we discuss our collected and calculated data and we show different explanations for dark matter.

2 Measuring Rotation Curves

For many years astronomers have developed methods in order to measure the rotation curves of spiral galaxies, as it is fundamental to determine the distribution of mass in a galaxy (Sofue 2001) in order to study its formation and evolution. Usually, absorption lines in the spectra are used. If the galaxy is rotating then the absorption lines will appear shifted due to the Doppler effect (Loelliet et al. 2014), which will allow us to deduce its rotation velocity, and from the velocity profile the mass distribution. These lines were first detected in 1914 by Silpher when he was analyzing the nuclear spectra of M31 and in the same year

Wolf (1914) detected shifted lines in the nuclear spectrum of M81. Later on, when technology improved, the strong emission lines of Hα and NII could be detected with spectrographs. Also the SII line was often used. Moreover, the HI (neutral hydrogen) line (at 21 cm) is very helpful when determining the rotation curves of galaxies, because its radial extent is much greater than the visible disk (Sofue 1996, Rubin, Ford & Thonnard 1980, 1982). Furthermore, hydrogen is the most abundant element in the Universe, and so it gives valuable information about galaxies. However, in the inner disk the HI is often weak or absent. This means that we have to use another line. Usually, CO lines in the millimeter wave range are the most useful (Kenney & Young 1988, Sofue & Nakai 1993). Carbon monoxide is emitted from molecular clouds that are found in star formation regions.

In order to measure the radial velocity of the Milky Way, maser lines have been used, such as SiO, OH and H_2O lines (Izumiura et al. 1995, Deguchi et al. 2000). Finally, for early type and complex galaxies where optical light is practically absent, planetary nebulae (PN) are used as tracers. A PN is a kind of emission nebula that consists of an expanding, glowing shell of ionized gas ejected from old red giant stars. Using the tools we have just described, the velocity of galaxies can be calculated using several different methods, such as the intensity-weighted-velocity method, the centroid-velocity and the peak-intensity-velocity methods, the envelope-tracing method and the iteration method (Sofue 2001).

3 Discrepancy between Theoretical and Real Rotation Curves

According to the luminosity-derived mass profile, if we make a plot of the rotational velocity of galaxies as a function of radius we would expect to see a Keplerian profile, i.e., the further away a point is from the center of the galaxy, the slower it rotates. The Keplerian profile can be deduced from applying Newton's laws to an orbiting planet (see Equations 1 and 2, where G is the gravitational constant, M the mass, r the radius and v the velocity):

$$G \cdot \left(\frac{Mm}{r^2}\right) = m \cdot \left(\frac{v^2}{r}\right), \tag{1}$$

$$v^2 = \frac{GM}{r}. \tag{2}$$

This is true if we consider constant the mass/luminosity ratio (which means that we suppose that all the mass inside the galaxy emits light). However, measurements that use the techniques explained in Section 2 showed that in reality at a certain radii the velocity does not decrease, but it becomes flat (Rubin et al. 1980, Bosma 1981, Faber & Gallagher 1979, Jimenez, Verde & Oh 2003, Cantinella, Giovanelli, Haynes 2006). This is called a flat rotation curve. At small radii the galaxy rotates and behaves as if it were a solid body. Then, when the profile should fall as if it were Keplerian, in fact it becomes flat and sometimes it even increases (see Figure 2).

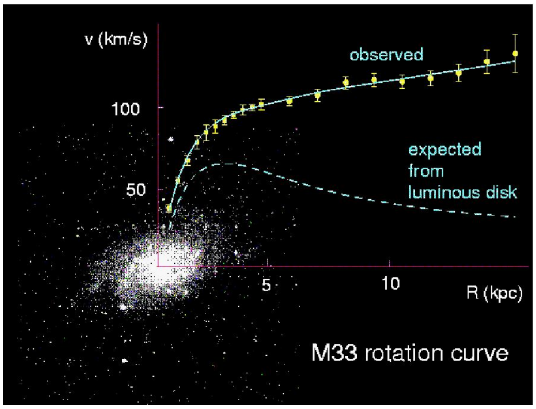

Figure 1: Scheme of the flat rotation curve of galaxies in comparison to the Keplerian profile (source: AstronomyNow).

As we already mentioned, according to the mass derived from luminosity, using the mass/luminosity relationship, the velocity should decrease with radius at large radii. Otherwise, if the velocity is kept constant or increases with the radius it could mean that there is more mass than the luminous one. Hence, we observe in galaxies that there is an substantial amount of mass which does not produce light, commonly known as *dark matter*. Many scientists have tried to get an analytical expression for the rotation curves of galaxies. Perhaps the most important contribution was made by Persic & Salucci (1991) when they proposed a Universal Rotation Curve. Other models have been proposed, which will be discussed in the next section.

4 Galaxy Models

When studying the kinetics of a galaxy we need to make some assumptions, as in most cases it is impossible to study them exactly as they are in reality. The process of making such assumptions is called modelization. The most known models are the following ones:

1. Point Mass: we model the galaxy as if it were a single point. The square of the velocity is obtained using this model can be seen in Equation 3, and the expression for the corresponding

gravitational potential is shown in Equation 4.

$$v^2(R) = GM/r, \tag{3}$$

$$\phi(R) = -\frac{GM}{r}. \tag{4}$$

2. Uniform Sphere: we model the galaxy as if it were a sphere. The square of the velocity is obtained using this model can be seen in Equation 5, the density profile is modeled in Equation 6 and the expression for the corresponding gravitational potential is shown in Equation 7.

$$v^2(R) = \frac{GMr^2}{2a^3}, \tag{5}$$

$$\rho(R) = \frac{3M}{4\pi a^3}, \tag{6}$$

$$\phi(R) = -\frac{3GM(a^2 - r^{2/3})}{2a^3}. \tag{7}$$

3. Isothermal sphere: The square of the velocity is obtained using this model can be seen in Equation 8, the density profile is modeled in Equation 9 and the expression for the corresponding gravitational potential is shown in Equation 10.

$$v^2(R) = 4\pi G\rho(0)a^2, \tag{8}$$

$$\rho(R) = \frac{\rho(0)}{(r/a)^2}, \tag{9}$$

$$\phi(R) = 4\pi G\rho(0)a^2 \ln(r/a). \tag{10}$$

4. Plummer Model: The square of the velocity is obtained using this model can be seen in Equation 11, the density profile is modeled in Equation 12 and the expression for the corresponding gravitational potential is shown in Equation 13.

$$v^2(R) = \frac{GMr^2}{(r^2 + a^2)^{3/2}}, \tag{11}$$

$$\rho(R) = \frac{3M/4\pi a^3}{(1 + (r/a)^2)^{5/2}}, \tag{12}$$

$$\phi(R) = -\frac{GM}{(r^2 + a^2)^{1/2}}. \tag{13}$$

5. Henriquist Model: The square of the velocity is obtained using this model can be seen in Equation 14, the density profile is modeled in Equation 15 and the expression for the corresponding gravitational potential is shown in Equation 16.

$$v^2(R) = \frac{GMr}{(r + a)^2}, \tag{14}$$

$$\rho(R) = \frac{(M/2\pi a^3)a^4}{r(r + a)^3}, \tag{15}$$

$$\phi(R) = -\frac{GM}{r + a}. \tag{16}$$

6. Jaffe Model: The square of the velocity is obtained using this model can be seen in Equation 17, the density profile is modeled in Equation 18 and the expression for the corresponding gravitational potential is shown in Equation 19.

$$v^2(R) = \frac{GM}{r + a}, \tag{17}$$

$$\rho(R) = \frac{(M/4\pi a^3)a^4}{r^2(r + a)^2}, \tag{18}$$

$$\phi(R) = \frac{GM}{a \ln(r/(r + a))}. \tag{19}$$

The Navarro-Frenk-White profile (NFW) is often used for N-body simulations (Navarro, Frenk & White, 1996). The density is modeled with the analytical expression shown in equation 20, where $\rho(0)$ and R_s (scale radius) are parameters that vary from halo to halo.

$$\rho(R) = \frac{\rho(0)}{\frac{r}{R_s}\left(1 + \frac{r}{R_s}\right)^2}.$$

However, we will not discuss these last two models or the isothermal sphere.

Regarding the other models, we make a comparison of the density profiles in Figure 2 and of the velocity profiles in Figure 3. We have considered the consant a to have a value of 1.

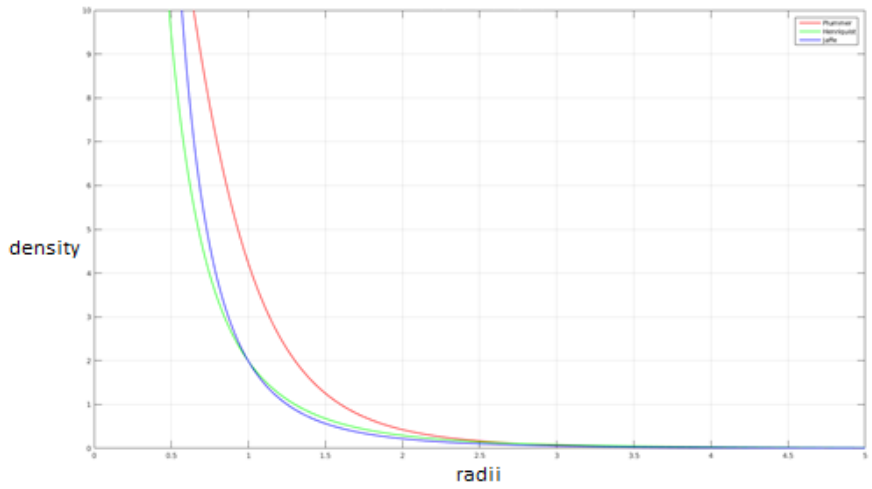

Figure 2: Different models of density profiles: in red the Plummer model, in green the Henriquist model and in blue the Jaffe model. Units are scaled from SI units.

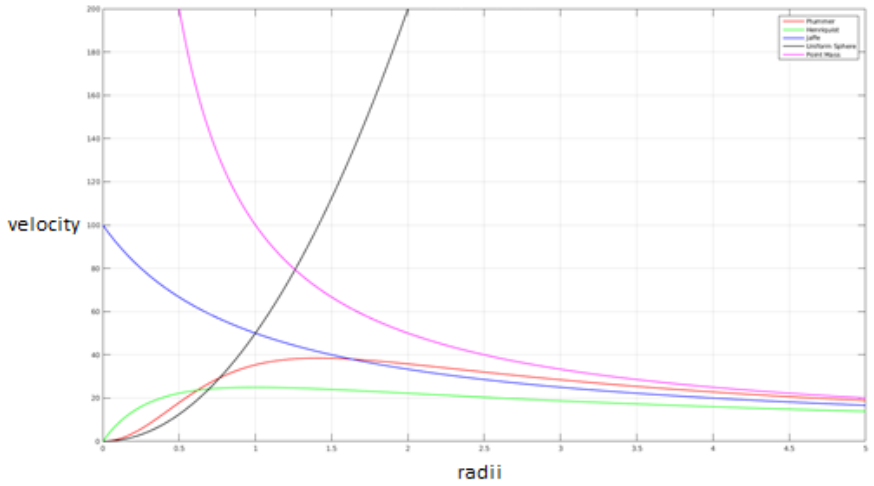

Figure 3: Comparison of the different velocity profiles: in red the Plummer Model, in green the Henriquist Model, in blue the Jaffe Model, in black the uniform sphere and in purple a point mass. Units are scaled from SI units.

5 Results

5.1 Experimental Data

Once we have described the different models, we proceed to compare them with real data. We have gathered information of 91 galaxies from the Updated Nearby Galaxy Catalog by the Astrophysics Science Division at NASA (Karachentsev et al. 2013). The information is presented in Table 2 in the Annex and includes the name of the galaxy, the major linear diameter (in kiloparsecs), the peak rotation velocity (using the HI line), the logarithm of the luminosity (in comparison to the luminosity of the Sun) and the logarithm of the mass enclosed in the Holmberg radius (in solar masses). Moreover, we have searched all the names of the galaxies in the webapage Simbad in order to know their morphological Hubble type. We describe all the parameters we include in the tables 1 and 2 as the Catalog defines them.

1. The major linear diameter: the major linear diameter, in kpc, at the Holmberg isophote of the galaxy.

2. The peak rotation velocity: the amplitude

$Vm = W50c/[2\sin(i)]$ of the rotational velocity of the galaxy, in km/s. This is adjusted for the inclination, where the HI line width, W50c, contains a correction for turbulent motions. W50 is the peak velocity of the galaxy.

3. The logarithm of the luminosity: the logarithm of the Ks band luminosity of the galaxy, in solar units, corrected for extinction and assuming an absolute magnitude of the Sun in the Ks band of 3.28.

4. The logarithm of the mass: the logarithm of the indicative mass M26 within the Holmberg radius of the galaxy, in solar masses, where M26 $= 3.31 \cdot 104 \cdot Vm_2 \cdot a26c \cdot D$, $a26c$ is the corrected angular diameter, in arcminutes, Vm is in km/s, and D is in Mpc.

The Holmberg radius is defined as the radius of the isophote of an elliptical galaxy corresponding to a surface brightness of 26.5 blue magnitudes per square arcsecond. The galaxies have been ordered according to their group: S, Sc, Sd, Scd, Sbc, Sa, Sm, Sp, SA, SB, SAB and S0. We have also separated the 91 galaxies in 4 groups: the non-barred galaxies (S, Sc, Sd, Scd, Sbc, Sa, Sm, Sp, SA), the barred galaxies (SB), the intermediate spiral galaxies (SAB) and the lenticular galaxies (S0). This way we can make comparisons depending on the morphology of each galaxy. We also include more information that we have calculated from this data.

We present the table of the average of the radii, the rotational velocity, the luminosity, the mass, the b, the a_0 of MOND, the mass/luminosity ratio and the percentage of missing mass for each type of morphological galaxy, and also for the barred, the non-barred, the SAB, the lenticular and the average of all the galaxies. The original data can be found in Table 2 in the Annex.

Type	Radius (kiloparsecs)	Vm (km/s)	logLk (solar units)	logMHi (solar masses)	b	a_0 MOND	M/L	%
Sc	6,33	60,67	8,90	8,82	9,65	1,83E-10	0,99	60,77
Sd	5,41	49,17	8,72	9,05	5,37	6,68E-11	1,04	29,34
Scd	7,69	79,33	9,42	8,88	12,05	3,87E-10	0,94	90,45
Sbc	10,00	156,00	10,60	10,08	11,49	7,96E-10	0,95	47,47
Sa	5,40	109,80	9,32	8,56	502,05	1,51E-07	0,93	38,05
Sm	5,74	64,67	9,21	8,93	6,12	1,53E-10	0,97	83,23
Sp	0,95	10,00	6,72	6,05	3,08	1,69E-11	0,91	48,17
SA	14,32	148,91	9,73	10,29	19,41	1,05E-09	1,00	26,23
SB	8,23	94,21	9,73	9,49	36663,78	1,12E-09	0,98	41,72
SAB	11,85	138,31	10,23	9,62	205116,37	2,50E-09	0,94	56,14
S0	6,40	94,75	9,77	8,48	408340,25	1,14E-09	0,87	92,94
unbarred	7,02	78,62	9,02	8,84	59,16	1,48E-08	0,98	46,76
barred	8,23	94,21	9,73	9,49	36663,78	1,12E-09	0,98	41,72
SAB	11,85	138,31	10,23	9,62	205116,37	2,50E-09	0,94	56,14
lenticular	6,40	94,75	9,77	8,48	408340,25	1,14E-09	0,87	92,94
all	8,09	93,08	9,42	9,09	61702,32	9,20E-09	0,97	49,39

Table 1: Average and calculated parameters for each morphological type of galaxy.

Then we want to check the percentage of missing mass. But firstly we have to make sure that our parameters are truly linked. We can see from the definitions that both the mass and the linear diameter (and hence the radii) are calculated inside the Holmberg radius. However, the W50 is the peak velocity (the maximum velocity in all the galaxy) and hence it is not the velocity at the Holmberg radius. This means that we have to make some calculations.

5.2 Peak radius

To do so, our first intention was to model the galaxy following a Keplerian profile. This way we would find the peak radius (that is, the radius in which we can find the peak velocity) by calculating where the derivative is 0. The Keplerian profile is defined as it can be seen in Equation 21. Then the function $M(r)$ can be modeled by integrating the density profile, which is defined as shown in Equation 22, where A is the total mass of the galaxy. We obtain Equations 22 and 23 and we differentiate them in Equation 24 and we equate it to 0 (in the peak the derivative has to be 0) and we solve for r in Equation 25.

$$v(R) = \sqrt{\frac{GM(r)}{r}}, \tag{20}$$

$$\rho(R) = Ae^{-r}, \tag{21}$$

$$M(R) = \int_0^r Ae^{-r}dr = A(1-e^{-r}), \tag{22}$$

$$v(R) = \sqrt{\frac{GA(1-e^{-r})}{r}}, \tag{23}$$

$$\frac{dv}{dr} = GAe^{-r}r - GA(1-e^{-r}), \tag{24}$$

$$e^{-r}r = 1 - e^{-r}. \tag{25}$$

But Equation 27 has only one solution: $r = 0$. We realize that in fact the Keplerian profile does not have any maximum and is always decreasing. The galaxy profile we were referring to is a combination of a solid body (in which the function is linear) and a Keplerian profile (which is a decreasing exponential). Precisely at the peak radius is where these two functions meet.

We note that the Jaffe model does not have any maximum either, but the Plummer and the Herniquist do. Figure 4 illustrates these functions.

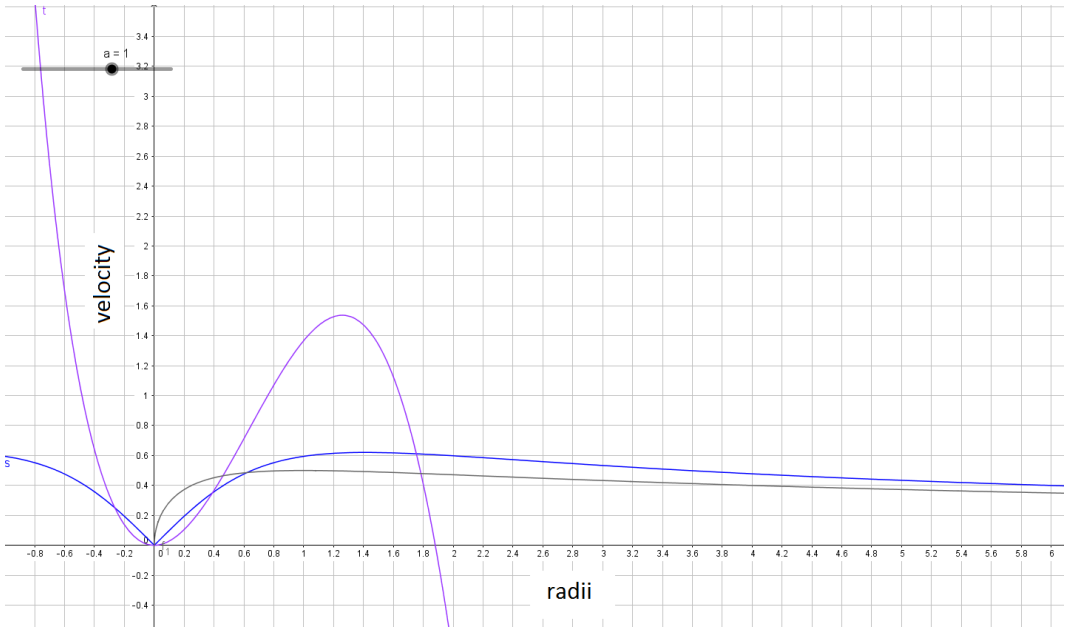

Figure 4: Plot of the Plummer velocity function (blue), of its derivative (purple) which crosses the x-axis not only at $r = 0$ and the Henriquist function (grey) which also has a maximum. Units are scaled from SI units.

We can apply the same process and we first differentiate the Plummer model (see Equation 26).

$$\frac{dv}{dr} = r^4e^{-r} + a^2r^2e^{-r} - r^3 + r^3e^{-r} + 2ra^2 - a^2 2re^{-r}. \tag{26}$$

If we equate Equation 26 to 0 and we consider the constant a to be 1 for simplicity and we obtain that $r = 1.8$.

5.3 Peak velocity

To obtain the maximum velocity from observations is not straightforward. In this work we use a sort of approximations to get it. Since we are working with flat rotation curves, we can assume that the peak velocity is mantained for all radii larger than the peak radius and hence also for the Holmberg radius. Using this simple approach we can compute the peak velocity and later on the missing mass of each galaxy (see following paragraphs). We have effectively checked that if we consider at the Holmberg radius as Keplerian profile and we compute the theoretical velocity, it is lower than the peak velocity. We consider the number b as it can be seen in Equation 27.

$$v_{\text{peak}} = \frac{GM}{r} \cdot b. \tag{27}$$

So b is the number for which we have to multiplicate the Keplerian velocity in order to get the real velocity. We can go one step further and compute the percentage of missing mass on each galaxy, that we define as M. We define x to be the difference between the two masses (see Equation 28).

$$x = \frac{vr}{G} - M. \tag{28}$$

And then we calculate the percentage of missing mass in Equation 29.

$$\frac{x}{M + x} \cdot 100. \tag{29}$$

Figure 12 is an scheme of how we compute the peak velocity and the difference between Keplerian and flat rotation curves. We assume that the inner region of the galaxy rotates like a rigid body until it encounters a Keplerian profile, and then it becomes flat. This is why we consider the velocity at the Holmberg radius to be the same as the peak velocity, because we

model it with a constant function. The velocity at the Holmberg radius following the constant velocity from the peak is higher than the velocity predicted by the Keplerian profile. This is because when the radius tends to an infinite value, the velocity according to the Keplerian profile tends to 0, whereas the flat rotation curve does not change its value. This difference between the two velocities evidentiates the amount of missing mass.

6 Modified Newtonian Dynamics

As an alternative to the theory of dark matter, Mordehai Milgrom proposed in 1983 another explanation of the missing mass in galaxies: the Modified Newtonian Dynamics (known as MOND). This theory proposes a modification of Newton's Laws, as shown in Equation 30, where F_N is the Newtonian force, m is the mass, a the acceleration, $\mu(x)$ a function (known as interpolating function) such that $\mu(x) \simeq 1$ for $x >> 1$ and $\mu(x) \simeq 1$ for $x << 1$.

$$F_N = m\mu\left(\frac{a}{a_0}\right)a. \tag{30}$$

The constant a_0 defines the critical acceleration at which Newton's Laws have to be modified in order to understand why there is mass missing. Then, when we apply MOND ($a << a_0$) we obtain the expression we show in Equation 31. If we apply this to a particle in a circular orbit we obtain the expression in Equation 32.

$$F_N = ma^2/a_0, \tag{31}$$

$$\frac{GMm}{r^2} = m\frac{(\frac{v^2}{r})^2}{a_0} \rightarrow v^4 = GMa_0. \tag{32}$$

We see that the velocity is independent from the radius, which makes sense because we are observing a flat rotation curve. This fits with the assumption we are making for our data. Hence, in Table 1 we also include the a_0 for each galaxy, which has been calculated with the mass and the velocity.

7 Discussion

Now we discuss about the data and the calculations we have carried on shown in Table 1 in Section 5.1. We must add that for all the parameters that we have calculated we have used units of the IS. Firstly, we will make some comments about relationships that can be established. Since we have compared and tested profiles for the radius-rotation velocity relation of galaxies, we show the full observational data in Figure 5.

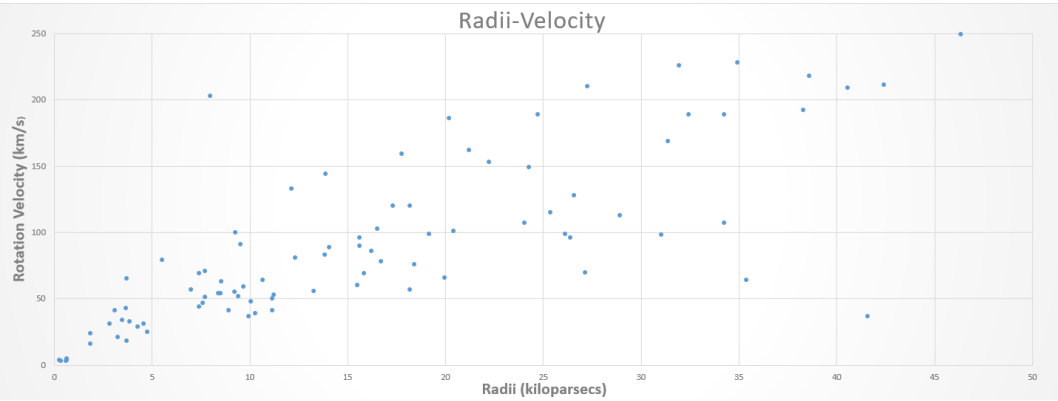

Figure 5: Comparison between the observed radii and the rotation velocity.

We see that until approximately 20 kpc the relationship is linear since in small galaxies the baryonic matter predominates. When the radii is bigger than this limit, the velocities of the different galaxies start diverging because dark matter dominates. This confirms the assumption that dark matter is more present in the outer regions of galaxies and that baryonic matter predominates in the innter regions. From 20 kpc, some velocities increase, some decrease and some are kept flat. This represent the various rotation curves of galaxies. Then, as we also observe that the luminosity and the mass are linked as it is shown in Figure 6.

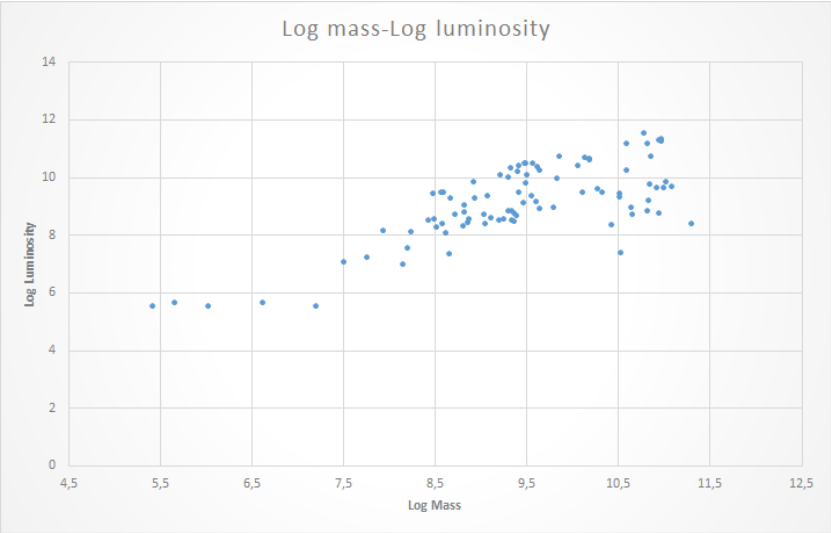

Figure 6: Comparison between the logarithm of the luminosity and the logarithm of the mass.

Although for this mass we are taking into account both baryonic and dark matter. This leads us to the idea that we can relate the luminosity of a galaxy and its rotation velocity (being aware that luminosity does not include dark matter), as it can be seen in Figure 7.

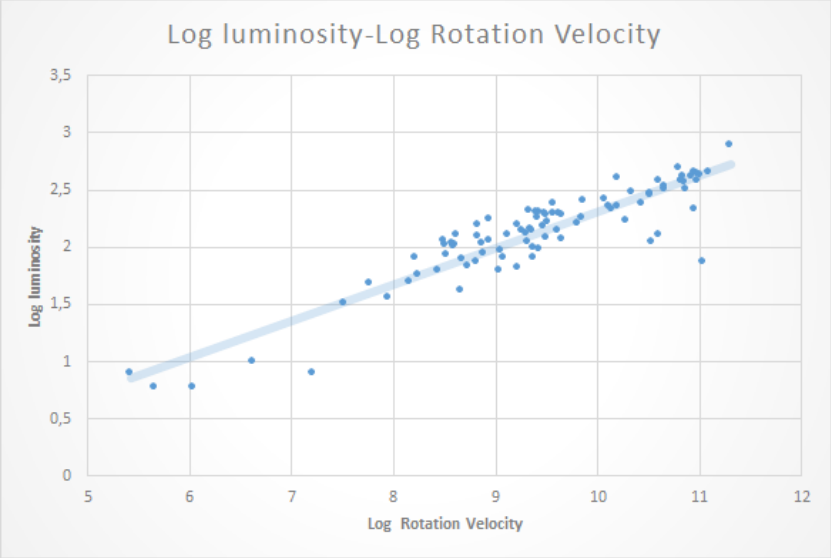

Figure 7: Comparison between the logarithm of the luminosity and the logarithm of the rotation velocity.

We can conclude that their relationship is linear. The gradient of the slope is 0.318 and the correlation coefficient is 0.83. This means that we can relate the total luminosity of a galaxy with its peak velocity or velocity at any point of the flat rotation curve. We find this particularly interesting since it might conform a way to find the rotation velocities of galaxies. Finally, we also observe that the mass/luminosity ratio is more or less similar for all radii, although there are differences (see Figure 8).

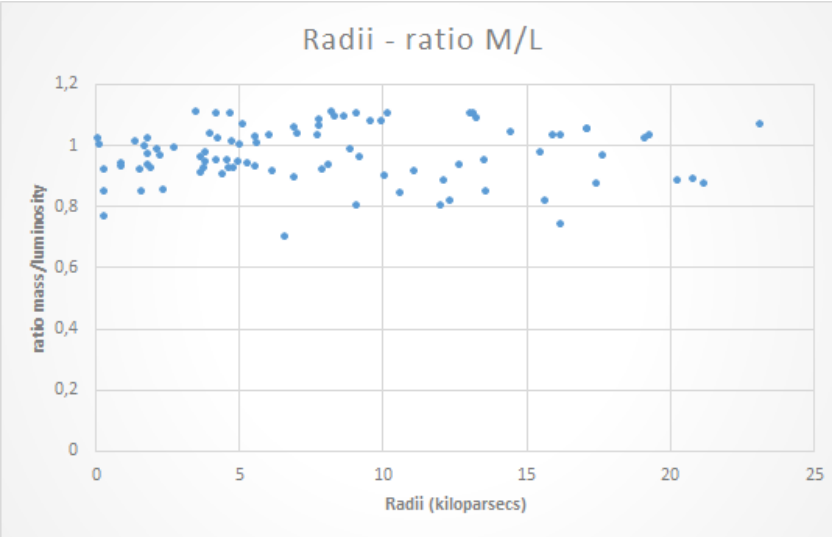

Figure 8: Comparison between the mass/luminosity ratio and the radii.

To compare the different morphological type of galaxies we ordered them according to values of their radius, peak velocity, luminosity and mass, in an increasing order.

Radius:
Sp/Sa/Sd/Sm/Sc/S0/Scd/SB/Sbc/SAB/SA

Peak velocity:
Sp/Sd/Sc/Sm/Scd/SB/S0/Sa/SAB/SA/Sbc

Luminosity:
Sp/Sd/Sc/Sm/Sa/Scd/SA-SB/S0/SAB/Sbc

Mass:
Sp/S0/Sa/Sc/Scd/Sm/Sd/SB/SAB/Sbc/SA

We observe various facts: the Sp type is always at the beginning of the comparison, i.e., less massive and smaller radius, which confirms the relationship of the four parameters. Either SA or Sbc are located at the end of the comparison and S0 is the one with the most strange behaviour, since it is the only one that seems not to follow the same pattern in all four comparisons. We must remark that S0 is in the limit between elliptical and spiral galaxies, and hence it is the most morphologically different galaxy. However, we do observe a distiction between barred and unbarred galaxies. In fact, if we look at the average values of the barred, unbarred, intermediate and lenticular galaxies the differences are huge. Barred galaxies are in average 1.21 kiloparsecs bigger than the unbarred, they rotate 15.95 km/s faster, their luminosity is 0.7 points higher and they are 0.63 points more massive. Also, their b parameter (the difference between a Keplerian curve and the reality) is also 36604 points higher. However, since they have more mass and velocity, they have a lower percentage of missing or dark matter: 46.75% for barred galaxies and 41.71% for unbarred galaxies. Their mass/luminosity ratio is approximately the same.

Surprisingly, the SAB galaxies, which are located between the barred and the unbarred galaxies, have all their parameters higher than both the barred and the unbarred galaxies. They are 4.82 kiloparsecs bigger than the unbarred galaxies, they rotate 59.60 km/s faster, their luminosity is 1.2 points higher and they are 0.78 points more massive. Also, their b parameter is much higher: 205057 points. Finally, their percentage of missing or dark matter is higher too: 56.14%. However, their mass/luminosity ratio is slightly lower: 0.94. As we mentioned, lenticular galaxies are not very regular: they are 0.61 kiloparsecs smaller than the unbarred galaxies yet they rotate 16.13 km/s faster. Their luminosity is 0.74 points higher than that of the unbarred and they are 0.35 points less massive. Nevertheless, their b parameter is extremely high, being 408281 points higher than that of the unbarred galaxies. This makes their percentage of missing mass to be also very high: 92.94%, whereas the other morphological types were not higher than 60%. Also, their mass/luminosity ratio is lower than the other 0.1 points. Also the Sa galaxy appears to have much less missing mass than the other types, as it is clear from its percentage and a_0 value.

Lastly, if we look at the average of all galaxies, we see that the missing mass represents a 49.38% in relation to the baryonic mass. We find this value to be optimal but low, since the percentage of estimated mass is calculated to be between 50 and 90%. Also, we see that the a_0 average value for the MOND constant is $9.19 \cdot 10^{-9}$ m/s, whereas Milgrom found $1.2 \cdot 10^{-10}$ m/s to be optimal. We can conclude that our value and the one found by Milgrom are very sim-

ilar. The a_0 we obtained is only 1.3% higher than the constant proposed by the MOND theory.

We can conclude that the two values are very similar, and although they are different in one order of magnitude, our value is almost 10.

8 Dark Matter

With our data we have found an average of 49.38% of missing mass in observed galaxies, which is widely thought to be dark matter. We now discuss the possible canditates for dark matter.

As we explained, dark matter dominates in the outer regions of galaxies. In fact, galaxies are thought to have another component: a dark matter inferred halo that surrounds the galaxy disk, beyond the visible parts of the galaxy (Donato, Gentile & Salucci 2004, Trujillo-Gómez et al. 2011). Normally, the density profile of the dark matter halo is modeled as shown in Equation 33, where r_c is the core radius (e.g. Coe 2010).

$$\rho(R) = \rho(0)\left(1 + \left(\frac{r}{r_c}\right)^2\right)^{-1}. \tag{33}$$

These halos could be formed by baryonic dark matter made originally from ordinary gas such as:

1. Molecular hydrogen gas clouds
2. Low mass stars or brown dwarfs
3. Stellar remnants: white dwarfs, neutron stars, black holes
4. Unknown elemental particles

These elements are known as MACHOs (MAssive Compact Halo Objects). Also cold molecular gas clouds made of hydrogen could apport mass although they do not emit light (Brandt 2016). We can also find non-baryonic explanations of dark matter, such as:

1. Massive neutrinos (Guetta et al. 2001)
2. Weakly Interacting Massive Particles (WIMPs): for instance the neutralino (Zhao et al. 2013)
3. Axions, which could interact electromagnetically (Graham & Rajendran 2013)

Observations have concluded that approximately 20% of the galactic halo is made of MACHOs and their typical mass is approximately 0.5 solar masses (Baum et al. 2016). This means that there are more white dwarfs than expected, since brown dwarfs are not that massive.

Usually there is also a distinction of whether the particles were created thermally in the early universe, or non-thermally in a phase transition. For instance, WIMP particles and neutrinos were created thermally, whereas axions are non-thermal. It is thought that when the universe was at very high temperatures, the number density of WIMPs was approximately equal to the density of photons. Then it cooled down and the creation of WIMPs became very rare. Also, supersymmetric particles are thought to conform dark matter. Supersymmetry relates bosons and fermions and if it existed all particles should have a symmetric partner. However, for now no partners have been found (source: Encyclopedia of Astronomy and Astrophysics). In opposition to the theory of dark matter, as we already mentioned Milgrom proposed the Modified Newtonian Dynamics. However, in the astrophysical community dark matter has a better acceptance.

9 Conclusions

After having presented our work we can summarize the following results.

1. A clear distinction can be made between the parameters we obtained for the unbarred, barred, intermediate and lenticular galaxies, being the barred bigger, more massive, and with higher luminosity and rotation velocities. The intermediate galaxies have been found to have all these parameters higher than both the barred and the unbarred. The mass/luminosity ratio of all the morphological types of galaxies did not differ much.
2. We established a linear relationship between the logarithm of the luminosity and the flat rotational velocities (km/s) of galaxies with a gradient of 0.318 and a correlation of 0.83.
3. The overall percentage of missing mass is found to be 49.38%, being much higher (92.94%) for lenticular galaxies.
4. We found an optimal value for the a_0 constant of the Modified Newtonian Dynamics to be $9.19 \cdot 10^{-9}$ m/s, which is only 1.3% higher than Milgrom's result of $1.2 \cdot 10^{-10}$ m/s.

10 Acknowledgements

Once this work is finished, I would like to thank in the first place the Joves i Ciència program from Fundació Catalunya la Pedrera for having allowed me to participate in this project. The two weeks we spent in Vall d'Àneu increased greatly my passion for science and

especially for astrophysics. I really enjoyed all the nights we spent star-gazing and I am very thankful for everything I lived and learned.

This experience has also allowed me to continue my scientific work through this article. I would like to thank my tutors Laia Casamiquela and Santi Roca-Fàbrega for their support and dedication, which has been fundamental. I only hope that this work will be the first of many.

11 Annexes

We here present the table which summarizes the collected data from the Updated Catalog of Nearby Galaxies, together with the C++ program which made the unit conversion and calculated our parameters and the Matplot program which made the graphics of the galaxy models.

```
#include<iostream>
#include<cmath>
#include <math.h>
using namespace std;

int main(){
cout<<"PLUMMER: radi,velocitat,massa"<<endl;
double G = 6.67/pow(10,11);
double M;
double x;
double r;
double v;
double v2;
double a = 1;
double formula;
double dif;
double b;
while(cin>>r>>v>>M){
M = pow(10,30)*1.9891*pow(10,M);
r = (r/2)*3.086*pow(10,19);
v = (v*1000)*(v*1000);
formula = (G*M)/r;
cout<<formula<<endl;
cout<<v<<endl;
dif = v - formula;
a = (v*r)/(G*M);
cout<<a<<"   ";
b = pow(v,4)/(G*M);
cout<<b<<endl;
cout<<"massa"<<endl;
x=((r*v)/G)-M;
cout<<"radi   "<<r<<"velocitat   "<<v<<"massa   "<<M<<"tot   "<<x<<endl;
cout<<x<<endl;
cout<<(x/(M+x))*100<<endl;
}
}
```

Figure 9: C++ program that calculates the parameters we included in the data.

```
N=100; %number of stars
m=1; %mass of a punctual star
M=N*m;
G=1;
a=1;

i=1;
j=1;
for r=0:0.1:5
   for phi=0:0.1:2*pi+0.1
      rho2DPlummer(i,j)=(3*M/(4*pi*a^3))./(1+(r/a).^2).^(5/2);
      rho2DHenry(i,j)=M/(2*pi*a^3)*a^4./(r.*(r+a).^3);
      rho2DJaffe(i,j)=M/(4*pi*a^3)*a^4./(r.^2.*(r+a).^2);
      rho2DSphere(i,j)=3*M/(4*pi*a^3);
      rho2DvPlummer(i,j)=G*M*r.^2./((r.^2.+a^2).^(3/2));
      rho2DvHenry(i,j)=G*M*r/((r+a).^2);
      rho2DvJaffe(i,j)=G*M./(r+a);
      rho2DvSphere(i,j)=G*M.*r.^2./(2*a^3);
      rho2DvPoint(i,j)=G*M./r;
      x(i,j)=r.*cos(phi);
      y(i,j)=r.*sin(phi);
      i=i+1;
   end
   j=j+1;
   i=1;
end

r=0:0.01:5;
phi=0:0.1:2*pi;
rho1DPlummer=(3*M/(4*pi*a^3))./(1+(r/a).^2).^(5/2);
rho1DHenry=M/(2*pi*a^3)*a^4./(r.*(r+a).^3);
rho1DJaffe=M/(4*pi*a^3)*a^4./(r.^2.*(r+a).^2);
rho1DSphere=3*M/(4*pi*a^3);
rho1DvPlummer=G*M*r.^2./((r.^2.+a^2).^(3/2));
rho1DvHenry=G*M.*r./((r+a).^2);
rho1DvJaffe=G*M./(r+a);
rho1DvSphere=G*M*r.^2./(2*a^3);
rho1DvPoint=G*M./r;
```

Figure 10: Matlab program that creates the plots of the mentioned models.

S	Type	Radii (kiloparsecs)	Vm: HI rot. Velocity (km/s)	logLk: Luminosity (solar masses)	logMHi: Mass within the Holmberg radius (solar masses)
IC2171	S	3,795	47	9,05	8,38
ESO495-008	S	1,84	43	8,52	8,26
UGC05672	S	4,975	37	8,81	8,31
AGC205278	S	0,925	16	7,51	7,06
Sc					
NGC0300	Sc	7,805	90	9,41	10,17
IC1959	Sc	3,5	57	8,49	9,42
NGC4236	Sc	13,57	70	9,61	9,14
IC3247	Sc	7,92	69	9,26	8,52
NGC4700	Sc	4,245	54	8,86	8,43
KUG 1202+28	Sc	0,93	24	7,76	7,22
Sd					
UGC01281	Sd	4,205	54	8,57	9,45
NGC0784	Sdm	5,15	39	8,67	9,26
ESO300-014	Sd	9,98	66	9,3	10
ESO300-016	Sd	1,86	18	7,94	8,12
IC2038	Sd	5,57	41	9,08	9,33
NGC1560	Sd	4,7	52	8,6	9,47
IC2233	Sd	8,345	78	9,22	10,07
UGC04704	Sdm	9,085	57	8,93	9,84
UGCA193	Sdm	5,615	53	8,5	8,55
ESO501-023	Sd	3,705	44	8,88	8,53
IC3077	Sd	2,385	25	8,16	6,97
NGC4534	Sd	4,28	63	8,82	9
Scd / Sdc					
UGC05923	Scd	3,7	69	9,35	8,49
NGC3413	Scd	3,86	71	9,34	8,83
UGC7321	Scd	15,51	98	9,56	9,33
Sbc		0			
Maffei2	Sbc	8,88	159	10,86	10,72
NGC3344	Sbc	11,12	153	10,33	9,44
Sa		0			
ESO483-013	Sa	1,745	34	8,72	8,68
NGC1800	Sa	2,295	31	9,04	8,7
ESO496-010	Sa	1,41	31	8,43	8,51
NGC4594	Sa	16,23	389	11,3	8,36
NGC4204	Sab D	5,325	64	9,12	8,57
Sm					
NGC1156	Sm	4,605	55	9,31	8,82
NGC2188	Sm	5,57	50	9,37	8,72
UGC03475	Sm	7,035	89	8,94	9,25
Sp					
NGC0855	Sp	4,455	41	9,37	8,45
And I	Sph	0,325	4	7,21	5,53
And XI	Sph	0,13	4	5,42	5,53
And XIV	Sph	0,305	3	6,03	5,53
And XIII	Sph	0,175	3	5,66	5,65
And V	Sph	0,33	5	6,62	5,62
SA					
NGC0045	SA	8,255	103	9,33	10,31
MESSIER031	SA(s)	23,17	249	10,79	11,52
MESSIER033	SA(s)	9,575	99	9,62	10,34
NGC0628	SA(s)	17,695	64	10,6	10,22
NGC0891	SA(s)	19,3	218	10,98	11,33
IC0342	SA(s)	17,125	189	10,6	11,15
NGC2552	SAm	6,915	83	9,51	10,05
MESSIER081	SA(s)	15,965	226	10,95	11,28
NGC3593	SA(s)	9,1	120	10,43	8,33
NGC4395	SA(s)	9,205	76	9,47	9,08
NGC5055	SA(rs)	21,205	211	11	9,62
SB					
IC1727	SB	7,745	60	9,49	9,8
NGC0672	SB(s)	7,815	96	9,65	10,22
NGC1291	SBa	20,795	37	11,03	9,82
NGC1313	SB(s)	8,65	120	9,57	10,46
NGC1744	SBd	10,205	101	9,42	10,38
LMC	SB(s)	5,03	48	9,42	9,44
NGC2500	SBd	6,155	81	9,8	8,95
NGC2537	SBm	4,77	91	9,84	9,96
NGC2541	SBc	13,055	99	9,48	10,47
NGC2835	SBc	14,45	113	10,19	10,63
NGC2787	SB(r)	3,995	203	10,19	10,58
NGC3109	SB(s)	3,865	51	8,58	8,38
UGC05427	SBd	1,555	41	8,21	7,54
NGC3351	SB(r)	10,6	162	10,65	8,94
NGC3556	SB(s)	6,93	144	10,52	9,42
NGC4490	SB(s)	8,105	86	10,28	9,59
UGC07678	SB	2,145	29	8,24	8,1
NGC4618	SB(rs)	4,84	59	9,65	8,9
NGC4945	SB(s)	15,68	169	10,66	8,71
SAB					
NGC0247	SAB(s)	13,195	96	9,5	10,45
NGC0253	SAB(s)	19,14	192	10,98	11,22
NGC0925	SAB(s)	17,125	107	10,14	10,66
NGC1637	SAB(rs)	6,06	133	10,07	10,4
NGC2403	SAB(s)	13,29	128	9,86	10,71
NGC2903	SAB(rs)	16,225	189	10,82	11,13
NGC3184	SAB(rs)	12,135	149	10,52	9,28
NGC3274	SAB(d)	2,765	79	8,83	8,76
NGC3368	SAB(rs)	13,625	210	10,83	9,18
NGC3489	SAB(rs)	6,63	56	10,53	7,36
NGC3521	SAB(rs)	17,46	228	11,09	9,65
NGC3627	SAB(s)	12,37	189	10,82	8,83
NGC4136	SAB(r)	4,635	100	9,39	8,67
NGC4258	SAB(s)	20,275	209	10,92	9,62
NGC4559	SAB(rc)	12,685	115	10,11	9,44
NGC4625	SAB(rs)	1,92	33	9,21	8,49
S0					
NGC0059	S0	1,63	21	8,66	7,34
NGC1533	S0	10,09	186	10,85	9,76
NGC1705	S0	1,855	65	8,62	8,06
NGC3115	S0	12,02	107	10,95	8,75

Table 2: Collected data from the Updated Catalog of Nearby Galaxies and Simbad.

References

[1] Baum, S., Visinelli, L., Freese, K., Stengel, P., arXiv:1611.09665.

[2] Bosma, A., 1981, AJ, 86, 1825.

[3] Bosma, A., 2016, 2016, IAU Symposium No. 321.

[4] Brandt, T., 2016, arXiv:1605.03665.

[5] Catinella, B., Giovanelli, R., Haynes, M.P., 2006, Astrophysics Journal.

[6] Coe, D., 2010, arXiv:1005.0411v1.

[7] Deguchi S., Fujii T., Izumiura H., Kameya O., Nakada Y., Nakashima J., Ootsubo T., Ukita N. 2000. Ap. J. Suppl. 128:571

[8] Donato, F., Gentile, G., Salucci, P., 2004, Mon. Not. Astron. Soc.

[9] Guetta, D., Spada, M., Waxman, E., 2001.

[10] Graham, P.W., Rajendran, S., 2013, Physical Review.

[11] Jimenez, R., Verde, L., Oh, S.P., 2003, MNRAS.

[12] Izumiura H., Deguchi S., Hashimoto O., Nakada Y., Onaka T., Ono T., Ukita N., Yamamura I. 1995. Ap. J. 453:837.

[13] Kenney, J & Young, S.J., 1988, ApJS, 66, 261.

[14] Loelliet, B., Bouchy, F., Deleuil, M., Royer, F., Bouret, J.C., Moutou, C., Barge, P., Laverny, P., Pont, F., Recio-Blanco, A., Santos, N.C., 2014, Astronomy & Astrophysics manuscript no. 7176.

[15] Milgrom, M., 2005, EAS Publication Series.

[16] Navarro, F., Frenk, S., White, D.M., 1996, Astrophysics Journal, 462:563.

[17] Persic, M., Salucci, P., Stel, F., 1999, Mon. Not. R. Astron. Soc.

[18] Rubin, V.C., Ford, W.K., & Thonnard, N., 1980, ApJ, 238, 471.

[19] Sellwood, J.A., Zánmar Sánchez, R., 2010, Mon. Not. Roy. Astron. Soc. 404, 1733.

[20] Sofue, Y., 1996, Astrophysics Journal, 458:120-131.

[21] Sofue, Y., 2001, Ann. Rev. Astron. & Astrophys. Vol. 39.

[22] Sofue, Y. & Nakai, N., 1993, PASJ, 45, 139.

[23] Trujillo-Gómez, S., Klypin, A., Primack, J., Romanowsky, J., 2011, Astrophysics Journal.

[24] Zhao, W., Yue, Q., Kang, K.J., Cheng, J.P., et al. 2013, arXiv:1601.04581.